AGU PUBLICATIONS

Geophysical Research Letters

RESEARCH LETTER

10.1002/2015GL066733

Key Points:
- Drifters at the surface respond similarly to cyclonic and anticyclonic forcing
- Subsurface drifters respond primarily to forcing that resonates with the ocean
- The wind coherence is very low between the inertial frequency and 1 cph

Correspondence to:
J. Röhrs,
johannes.rohrs@met.no

Citation:
Röhrs, J., and K. H. Christensen (2015), Drift in the uppermost part of the ocean, *Geophys. Res. Lett.*, *42*, 10,349–10,356, doi:10.1002/2015GL066733.

Received 24 OCT 2015
Accepted 9 NOV 2015
Accepted article online 13 NOV 2015
Published online 2 DEC 2015

Drift in the uppermost part of the ocean

Johannes Röhrs[1] and Kai H. Christensen[2]

[1]Norwegian Meteorological Institute, Bergen, Norway, [2]Norwegian Meteorological Institute, Oslo, Norway

Abstract Lagrangian drift velocities within the uppermost meter of the ocean mostly depend on the local wind forcing, turbulent mixing, and waves. While the interior part of the Ekman layer has been extensively studied using drogued drifters, the drift at—or very close to—the surface is less investigated. The wind response of surface currents on time scales from 1 h to 10 days is analyzed using two types of satellite-tracked drifters: (i) spherical floats on the surface and (ii) drifters with a drogue centered at 70 cm depth. The response of drifting objects to wind and wave forcing is highly dependent on the vertical position, even within the upper meter of the ocean. The surface drifters are wind coherent for both cyclonic and anticyclonic subinertial frequencies. In contrast, the subsurface drift responds primarily to anticyclonic forcing that resonates with the intrinsic ocean dynamics.

1. Introduction

Accurate models of the drift in the uppermost part of the ocean—from the surface and down to a few meters depth—play a crucial role in operational oceanography, for example, as support for search-and-rescue operations or remedial action in connection with oil spills. The ocean currents here are largely controlled by atmospheric forcing, turbulent mixing, and waves. An understanding of how any floating object is exposed to these mechanisms is crucial to predict its drift.

The drift of floating objects and the deflection angle between the wind and the surface current is a long-standing problem. *Ekman* [1905] showed that the deflection angle is 45° when the eddy viscosity is held constant with depth. *Gonella* [1972] extended the Ekman theory by allowing for a depth-dependent viscosity and yield a deflection angle between 45 and 90°, assuming a well-mixed upper layer that slides with no friction on the deeper layers. If mixing is limited near the surface, deflection angles reduce to 10–40° [*Weber*, 1983; *Ardhuin et al.*, 2009]. Hence, the surface drift deflection angle is very sensitive to both the effective viscosity and the stratification, and one can expect large variations depending on the regional and seasonal climate [*Rio and Hernandez*, 2003].

The drift in the uppermost layer is furthermore affected by surface waves [e.g., *Rascle and Ardhuin*, 2009; *Röhrs et al.*, 2012]. Objects in the upper few meters are exposed to the wave-induced Stokes drift [*Stokes*, 1847; *Monismith and Fong*, 2004; *Röhrs et al.*, 2014]. In addition, dissipation of wave momentum [e.g., *Carniel et al.*, 2009; *Christensen and Terrile*, 2009] and the interaction of wave momentum with planetary vorticity (the so-called Coriolis-Stokes force [*Ursell*, 1950; *Hasselmann*, 1970]) alter the underlying Eulerian currents. For example, *Lewis and Belcher* [2004] show that the Coriolis-Stokes force deflects the surface current by about 10°–20° farther to the right (Northern Hemisphere) compared to the classic steady Ekman balance (see also *Polton et al.* [2005]). In addition, surface waves influence the upper ocean mixing by injection of turbulence kinetic energy and through Langmuir turbulence and Stokes drift shear [*Janssen*, 2012; *McWilliams et al.*, 2012; *Drivdal et al.*, 2014; *Babanin et al.*, 2012]. Such wave effects are not included in classical Ekman models, but they are inevitably included in all field observations and should be considered when interpreting field data [*Pazan and Niiler*, 2001; *Röhrs et al.*, 2012].

Satellite-tracked drifters have proven useful to assess wind-driven currents, because they can sample an extended region with reasonable logistical effort [*Lumpkin and Pazos*, 2007; *Poulain et al.*, 2013]. Rotary cross-spectral analysis of winds and currents provides a means for separating (i) the ocean response to atmospheric forcing and (ii) tides and inertial oscillations. This procedure was pioneered by *Gonella* [1972] who used data from moored current meters. *Niiler and Paduan* [1995] made a similar analysis of Lagrangian data using drifters from the surface velocity program (SVP).

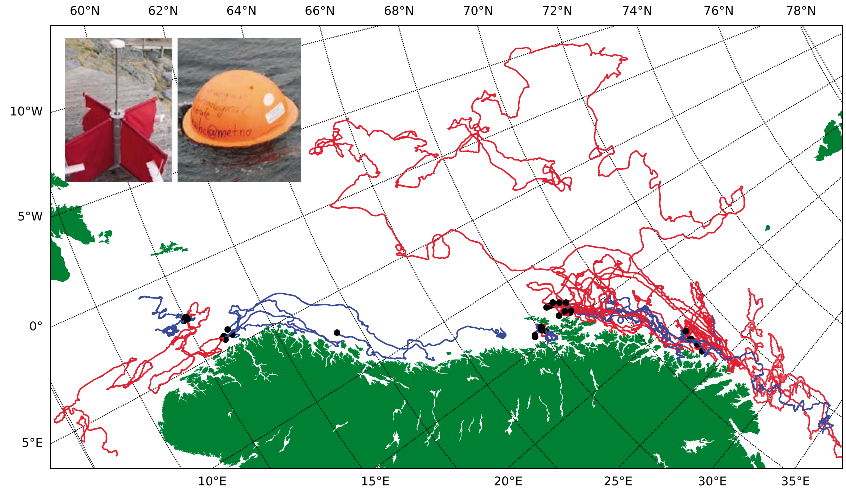

Figure 1. The trajectories of the CODE drifters (blue) and iSphere drifters (red) used in this study. A total amount of 25 CODE and 41 iSphere drifters are used, providing 405 and 1072 drifter days, respectively. The inset photographs show (left) CODE and (right) iSphere drifters.

Experiments with SVP drifters have provided knowledge about horizontal dispersion and wind-induced drift in the interior of the Ekman layer [e.g., *Koszalka et al.*, 2009; *Poulain et al.*, 2013]. The Ekman depth and effective viscosities can be determined by fitting idealized Ekman-type models to observed drifter velocities and wind reanalyses [e.g., *Niiler and Paduan*, 1995; *Rio and Hernandez*, 2003]. The deflection angle of wind-induced currents at the average drogue depth (15 m for SVPs) has been found to be 70° [*Niiler and Paduan*, 1995] in the northeast Pacific and between 27 and 42° in the Eastern Mediterranean [*Poulain et al.*, 2009]. In a global study, *Rio and Hernandez* [2003] have mapped the deflection angle for summer and winter, reporting values ranging from 20° to 60° for most regions.

While the currents in the interior of the mixed layer have been extensively studied using SVP drifters and moored current meters, knowledge about the variability in the upper few meters is lacking. The presence of surface waves complicates acoustic measurements [*McWilliams et al.*, 2012], and the influence of the Stokes drift near the surface requires that drifter trajectories are interpreted in a Lagrangian framework [*Röhrs et al.*, 2012].

We extend previous investigations by analyzing how drifters at or near the surface respond to wind forcing at time scales from 1 h up to 10 days. The analysis is based on rotary spectral analysis, and we compare the frequency distributions of the cyclonic and anticyclonic drift velocity components for two different drifter types. In addition, we discuss the wind and drift velocity rotary cross spectra in some detail. Central to our results are the rotary cross-spectra coherence and admittance values: the coherence expresses how well the wind and drift velocity time series are in phase, while the admittance is a measure of the correlation in amplitude of the rotary components.

2. Data and Methods

Trajectories from two different drifter types (Figure 1) are used to analyze the drift in the uppermost part of the ocean: (i) iSphere drifters and (ii) drifters using the Coastal Ocean Dynamics Experiments (CODE) design [*Davis*, 1985].

iSpheres have a slightly flattened spherical shape (39 cm horizontal diameter and 31 cm height) and do not have a drogue. They are half submerged in water such that the airside and waterside cross-section areas are the same. Since they are aerodynamically smooth, the wind drag accounts for only one third of the leeway, while the rest is due to the Stokes drift and the wind-induced Eulerian currents [*Röhrs et al.*, 2012].

CODE drifters consist of a cross-shaped drouge of one 71 cm height and 51 cm width, centered at 64 cm depth. It is stabilized by four flotation elements and has an antenna that protrudes through the surface. Its cross-section area of water versus air elements is about 40; hence, the wind drag is small [*Davis*, 1985].

A total number of 66 drifters were deployed in the Norwegian Sea and the Barents Sea during 2010–2015 (Figure 1), amounting to a total of 405 CODE drifter days and 1072 iSphere drifter days. Drifter positions are provided every 30 min by the Global Positioning System and reported using Iridium telemetry. Drifter velocities are given by the position increments, representing 30 min averages. The drifters used for this study were produced by MetOcean, Canada.

Surface winds are taken from the NORA10 archive, which is a downscaling of the ERA-40 Reanalysis for the Northeast Atlantic [*Reistad et al.*, 2011]. For the years after 2002, NORA10 is being continued using operational analyses from the European Centre for Medium Range Weather Forecasts and provides hourly winds with 10 km resolution [*Aarnes et al.*, 2012]. Marine boundary layer winds from NORA10 validate well against in situ observations from offshore platforms and rawinsondes [*Furevik and Haakenstad*, 2012]. NORA10 winds at 10 m height were bilinearly interpolated to the drifter positions.

The NORA10 archive includes a wave hindcast, which is used to assess the surface Stokes drift and integrated wave parameters. From these, we calculate Stokes drift at 1 m depth using the approximated Stokes drift profiles derived by Ø. Breivik et al. (A stokes drift approximation based on the phillips spectrum, submitted to *Ocean Modelling*, 2015).

Following *Gonella* [1972], we represent drifter velocities by spectra of rotary components. The eastward and northward velocities (u_x, u_y) are written in complex form such that $u(t) = u_x + iu_y$, with Fourier transform $\mathcal{F}(u) = \hat{u}(\omega)$. The rotary spectrum of $u(t)$ is then

$$S_{uu}(\omega) = \frac{1}{N\Delta t} < \hat{u}^* \hat{u} >, \tag{1}$$

where negative frequencies represent anticyclonic components and positive frequencies represent cyclonic components. In our analysis $\Delta t = 0.5$ h is the sampling rate and the brackets $<\cdot>$ denote a block average, where the time series $u(t)$ has been split up in blocks of $N = 512$ samples (approximately 11 days) with 50% overlap. The mean is substracted from each block and a Hamming window applied to reduce spectral leakage [*Emery and Thomson*, 1997].

We further calculate rotary cross spectra between wind and drifter velocities:

$$S_{wu}(\omega) = \frac{1}{N\Delta t} < \hat{w}^* \hat{u} >, \tag{2}$$

where $\hat{w}$ is the Fourier transform of the complex wind velocity $w(t)$ [e.g., *Niiler and Paduan*, 1995]. The coherence, a measure of how well two time series are in phase, between wind and drifter velocities is

$$\gamma^2_{wu}(\omega) = \frac{|S_{wu}|^2}{S_{uu}S_{ww}}. \tag{3}$$

The admittance, which relates the drifter velocity to the wind as forcing agent, is

$$Z_{wu}(\omega) = \frac{S_{wu}}{S_{ww}}, \tag{4}$$

where S_{ww} is the rotary spectra of the wind. It follows from equations (2) and (4) that the admittance for a particular frequency scales like the ratio of drifter and wind speeds:

$$|Z_{wu}|(\omega) \sim \left(\frac{|u|}{|w|} \right) \bigg|_{\omega}, \tag{5}$$

where $|u|$ and $|w|$ represent the drift and wind speeds for the Fourier components with frequency ω.

For a more common estimate of the drifters leeway and deflection angle we also calculate the complex correlation coefficient between wind and drifter velocities as defined by *Kundu* [1976]:

$$R = \frac{< u'^* w' >}{\sqrt{< u'^* u' > < w'^* w' >}} \tag{6}$$

with $u' = u - \overline{u}$ and $w' = w - \overline{w}$, where $\overline{u}$ and $\overline{w}$ denote averages over one block of length N.

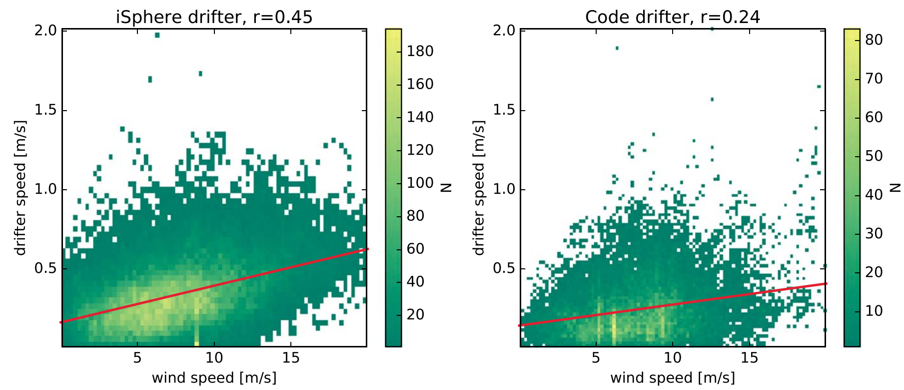

Figure 2. Two-dimensional histogram of wind speed versus drifter speed for (a) iSphere drifters and (b) CODE drifters. The red lines represent linear regressions between wind and drifter speed.

3. Results

The average drifter speeds during this experiment were 32 cm/s (iSphere) and 22 cm/s (CODE). The average wind speed along the drifter trajectories was 7.5 m/s. The average Stokes drift was 8.9 cm/s at the surface, and 3.7 cm/s at 1 m depth.

Prior to presenting the rotary spectral analysis, we briefly investigate the correlation between drifter and wind speeds. The drift speed of both drifter types are correlated with wind speed to within the 99% significance level. The correlation coefficients are very low however, particularly for the CODE drifters. Hence, the drift velocities cannot be predicted from wind data only (compare Figure 2). Correlation coefficients and linear regression slopes are given in Table 1. The phases of the complex correlation coefficients represent the average deflection angles between drifter velocities and the wind velocity, which are 62° (iSphere) and 73° (CODE) to the right of the wind.

The rotary spectra of the drifter velocities are shown in Figure 3. Both drifter types show a decay of energy toward higher frequencies and a distinct peak near the inertial and the tidal M2 frequency (which are very similar in this region). This result is consistent with previous experiments [e.g., *Elipot and Gille*, 2009a; *Poulain et al.*, 2013].

The rotary spectra reveal distinct differences in drift behavior above and below the diurnal frequency. For the low frequencies, the anticyclonic and cyclonic components of both drifter types have the same energy densities, but the two drifter types behave differently; the iSphere drift velocities contain about twice as much energy compared to the CODE drifters. For the high frequencies, the energy levels of the two drifter types are strikingly similar, but the anticyclonic components contain more energy than the cyclonic.

Since inertial motion is anticyclonic, the narrow peak for the cyclonic components at $\omega \approx 12^{-1}$ cph is due to the tides. The broader peak in the energy density of the anticyclonic components indicates the presence of

Table 1. Correlation Coefficients (r) Between Wind Speed ($|w|$) and Drifter Speed ($|u|$) and the Slope (s) of the Linear Regression Shown in Figure 2[a]

	iSphere	CODE
r	0.45	0.24
s	2.3%	1.3%
$\|R\|$	0.74	0.51
Phase (R)	62°	73°
$\|Z_{wu}\|$	3.22%[b]	2.43%[b]
Phase (Z_{wu})	64°[b]	84°[b]

[a] R is the complex correlation coefficient between u and w and Z_{wu} is the admittance spectra.
[b] Average over all frequencies where the cross spectrum coherence is above the confidence limit (compare Figure 4).

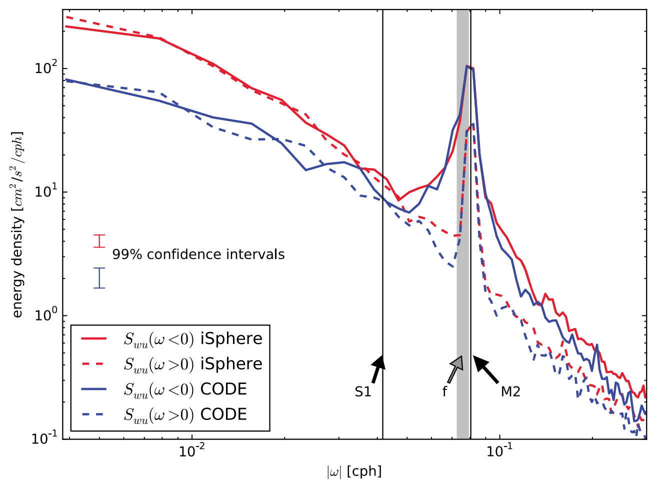

Figure 3. Rotary spectra of iSphere and CODE drifter velocities. Dashed lines show the cyclonic and solid lines the anticyclonic rotating components. The range of the Coriolis parameter f in the domain of the drifter data is indicated in gray shading. Vertical lines show the frequencies of the diurnal tide S1 and the semidiurnal tide M2. The confidence intervals are based on the degrees of freedom determined by the number of raw spectra used for the analysis.

near-inertial oscillations [*Poulain et al.*, 2013], which are expected to occur over a range of frequencies near the inertial frequency, f [*Crawford and Large*, 1996].

Figure 4 (top) shows the coherence between the wind and the drifter velocities. For the iSpheres, the coherence increases for decreasing frequencies between $\pm 12^{-1}$ cph. In contrast, the CODE drifter velocities are primarily coherent with the wind for anticyclonic components, and overall coherence values are lower than for the iSpheres. The minima around $\pm 12^{-1}$ cph coincide with the peaks in the rotary spectra (Figure 3), which shows that drift velocities at these frequencies are primarily due to inertial oscillations and tides.

Spectra of absolute admittance are shown in Figure 4 (middle). The admittance for the iSphere drift velocities has a flat plateau where the coherence is above the confidence limit. In this region, the amplitudes of surface drift compared to wind speed has no frequency dependence, equivalent to a leeway of about 3.2%. The strongest response in amplitude is around the inertial frequency $\omega \approx -f$ regardless of the signals not being in phase (low coherence), which is particularly noticeable for the CODE drifter velocities. Average admittance values for coherent frequencies are presented in Table 1.

Figure 4 (bottom) shows the phases of the rotary cross spectra S_{wu}, which are equivalent to the deflection angles between the wind and the drifter velocities. The deflection angles are between 60 and 80° for most low-frequency components ($|\omega|<12^{-1}$ cph, see also Table 1). The CODE drifter deflection angles are more scattered in the cyclonic components between $24^{-1} < \omega < 12^{-1}$ cph. The phase of S_{wu} has no significance where the coherence drops below the confidence limit ($|\omega| > 12^{-1}$ cph).

4. Discussion

4.1. Time Scales for Surface Drift

The analysis covers time scales from about 10 days to 1 h, thereby complementing previous studies of global data with lower resolution [e.g., *Rio and Hernandez*, 2003; *Elipot and Gille*, 2009a]. Our data confirms the conjecture of *Rio and Hernandez* [2003] that wind coherence for surface drifters vanishes between the inertial and the Nyquist frequency (1 cph, Figure 4, top). It is possible that the wind coherence increases again at even shorter time scales, but no conclusions can be made from our data. *Poulain et al.* [2009] found a maximum wind coherence for CODE type drifters and undrogued SVPs for periods of 3–10 days. We also find increasing coherence for decreasing frequencies, with a maximum at 10 days, which is the longest period investigated in this study.

At low frequencies, the iSphere drift velocities are more energetic than the CODE drift velocities (Figure 3), which is a result of the iSpheres being exposed directly to the large-scale forcing of the wind and the Stokes drift. At the depth of the CODE drifter, the average Stokes drift is reduced by more than 50% compared to the surface. Being less exposed to wind and the Stokes drift, the CODE drifters are primarily driven by the

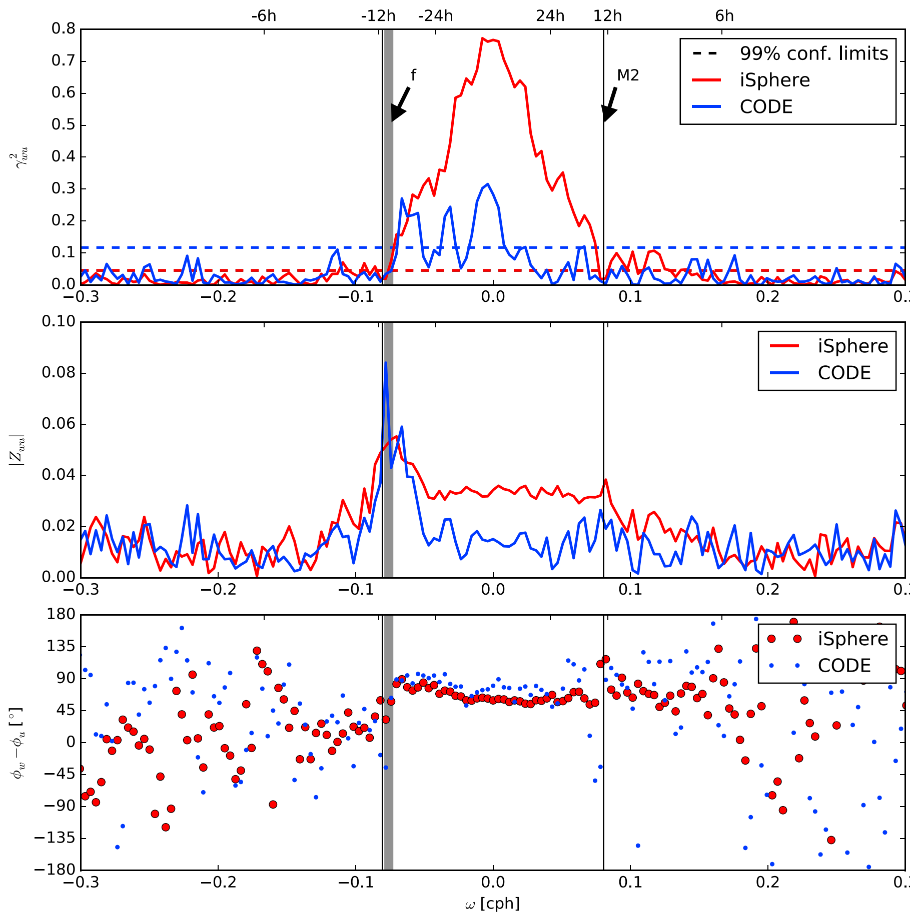

Figure 4. (top) Coherence spectra of wind and drifter velocities, with negative frequencies representing anticyclonic rotary components. The confidence limits are given by the equivalent degrees of freedom used for each spectral estimate [*Emery and Thomson*, 1997]. (middle) Admittance spectra for the response of drifter velocity to wind. (bottom) Phase angle of the rotary cross spectra.

Eulerian surface currents. At near-inertial frequencies, where surface currents are dominated by the intrinsic ocean dynamics, the energy density spectra of both drifter types are similar.

The coherence spectra exceed the confidence limit only when the drifter velocities have a well-defined phase relative to the wind, which occurs for frequencies below $|f|$ (Figure 4, top). For shorter time scales, the boundary layer is seldom in a steady state with the forcing. In particular, near the inertial frequency the drift is not wind coherent. Nevertheless, Figure 4 (middle) shows maximum admittance for both drifter types near the inertial frequency. Hence, the surface currents resonate with winds that rotate at approximately the inertial frequency, as shown in numerical experiments by *Crawford and Large* [1996].

The asymmetry in CODE drifter coherence values is due to the fact that only anticyclonic waves are trapped by planetary vorticity in the Ekman layer [*Gonella*, 1972]. Since iSpheres are directly exposed to wind and waves, their velocities can reach a steady state for both cyclonic and anticyclonic winds, while the CODE drift only becomes wind coherent for anticyclonic forcing when the Ekman layer can resonate with the wind.

4.2. Leeway

Our results for the leeway (Table 1) generally agree with the experiment by *Poulain et al.* [2009], who found a ratio of 2% for undrogued SVP drifters (compared with 2.3% for the iSpheres in this study) and a ratio of 1% for CODE drifters (compared with 1.3% in this study). The magnitude of the admittance $|Z_{wu}|$ expresses a frequency-dependent leeway (cf. equation (4)). The average admittance for the iSpheres at coherent frequencies is 3.0–5.0%, similar to leeway factors typically used in oil spill drift modeling [e.g., *Drivdal et al.*, 2014]. Comparing with the lower values for the CODE drifters, we argue that the major difference in the leeway for the two drifter types are due to the impact of wind drag and Stokes drift on the iSpheres, with the latter being the most important [*Röhrs et al.*, 2012].

4.3. Drift Deflection Angle

The deflection angle for the iSphere drifters at coherent frequencies is 64°, given by the phase of the cross spectra S_{wu} (Figure 4, bottom). A comparable value of 62° is given by the phase of the complex correlation of the raw time series. The CODE drifters have a deflection angle of 84° as obtained from the cross spectra, compared to 73° from the complex correlation. A similar value for the surface deflection angle (60°) has also been found by *Niiler and Paduan* [1995] using a regression model for the Ekman layer fitted to observations.

The observed deflection angles and their frequency dependence are also in the range of possible Eulerian surface currents calculated from the extended Ekman model of *Gonella* [1972]. In this model, the drift at the surface should be 90° to the right of the wind at a frequency of $\omega = -f$, decaying to 45° for $\omega > f$ which compares well with the frequency dependence of iSphere drift deflection angles observed here (Figure 4, bottom). A corresponding frequency dependence has also been observed for SVP drifters in the Southern Hemisphere [*Elipot and Gille*, 2009b, Figure 5]. In contrast to Gonella's model, our iSphere drifters are also affected by the Stokes drift, which could explain the lower deflection angles particularly for high-frequency forcing.

4.4. Regional Sensitivity

The deflection angles obtained in this study differ from those of *Poulain et al.* [2009], who reported values between 17 and 20° for undrogued SVP drifters that are identical to iSpheres and 28° for CODE drifters deployed in the Mediterranean. *Poulain et al.* [2009] also reported 27–42° deflection angles for drogued SVP drifters, as opposed to 70° reported by *Niiler and Paduan* [1995]. A possible explanation for these discrepancies is increased stratification in the Mediterranean, which would disconnect the upper layer from the ocean interior by inhibiting vertical mixing. This comparison suggests a strong dependence of the deflection angle on the vertical structure of the mixed layer, which again depends on the regional and seasonal climate [*Rio and Hernandez*, 2003].

A part of the here used drifter trajectories are in close proximity to the coast, and their mean drift are to a greater extent influenced by topography, which appears as more noise in the rotary cross spectra. A sensivity test, where trajectory segments that are closer than 50 km to the coastline have been removed, yielding the same general behavior in the coherence, admittance, and phase spectra for both drifter types. Values for the leeway were roughly the same, but the wind deflection angle was 3° larger for iSphere drifters and 10° larger for the CODE drifters. Using high-frequency radar observations, *Fontán and Cornuelle* [2015] show how the wind response of surface currents is modified near coastalines by polarizing inertial oscillations.

While the quantitative results for the leeway and deflection angles reflect local conditions, we expect that the qualitative differences between surface drift and drift at 1 m depth and low wind coherence above the inertial frequency should apply elsewhere.

4.5. Concluding Remarks

Both the CODE and the iSphere drifters represent the drift in the uppermost part of the ocean. Their response to atmospheric forcing is very different, partly because of their vertical position and partly because of different airside and waterside drag ratios. The deflection angles of the CODE drifters are about 10–20° farther to the right of the wind and their overall drift speeds are lower, in particular, on time scales longer than a day. The major difference between iSphere and CODE drifters is the exposure to wind and waves, which causes the iSpheres to have smaller wind deflection angles. The CODE drifters experience only little wind drag and the Stokes drift, which decays rapidly with depth, is less relevant for CODE drifters [*Davis*, 1985; *Röhrs et al.*, 2015].

It is clear that both wind and wave data are crucial for correctly modeling upper ocean drift, but since the drift velocities are not wind coherent on frequencies between the inertial period and 1 cph, short-term forecasts require explicit models for the ocean circulation and, in particular, the Ekman layer response to the atmospheric forcing.

In addition, it is important to know the vertical position of the drifting objects or the vertical distribution if considering buoyant material such as oil droplets. Modeling upper ocean drift and the vertical distribution of buoyant material requires accurate mixing schemes for the uppermost part of the ocean, which is one of the major challenges in operational oceanography today.

Acknowledgments
The drifter data will be provided upon request to the corresponding author. The NORA10 data used here are available on request to the Norwegian Meteorological Institute. This work was financed by the Research Council of Norway (RCN) through grant 244262 (RETROSPECT). The drifters were sponsored and deployed through the RCN grants 196438 and 207541 as well as by the Norwegian Clean Seas Association and the Royal Norwegian Navy.

References

Aarnes, O. J., Ø. Breivik, and M. Reistad (2012), Wave extremes in the Northeast Atlantic, *J. Clim.*, *25*, 1529–1543, doi:10.1175/JCLI-D-11-00132.1.

Ardhuin, F., L. Marie, N. Rascle, P. Forget, and A. Roland (2009), Observation and estimation of Lagrangian, Stokes, and Eulerian currents induced by wind and waves at the sea surface, *J. Phys. Oceanogr.*, *39*(11), 2820–2838, doi:10.1175/2009JPO4169.1.

Babanin, A. V., M. Onorato, and F. Qiao (2012), Surface waves and wave-coupled effects in lower atmosphere and upper ocean, *J. Geophys. Res.*, *117*, C00J01, doi:10.1029/2012JC007932.

Carniel, S., J. Warner, J. Chiggiato, and M. Sclavo (2009), Investigating the impact of surface wave breaking on modeling the trajectories of drifters in the northern Adriatic Sea during a wind-storm event, *Ocean Modell.*, *30*(2–3), 225–239, doi:10.1016/j.ocemod.2009.07.001.

Christensen, K. H., and E. Terrile (2009), Drift and deformation of oil slicks due to surface waves, *J. Fluid Mech.*, *620*, 313–332, doi:10.1017/S0022112008004606.

Crawford, G. B., and W. G. Large (1996), A numerical investigation of resonant inertial response of the ocean to wind forcing, *J. Phys. Oceanogr.*, *26*, 873–891, doi:10.1175/1520-0485(1996)026<0873:ANIORI>2.0.CO;2.

Davis, R. E. (1985), Drifter observations of coastal surface currents during CODE: The method and descriptive view, *J. Geophys. Res.*, *90*(C3), 4741–4755, doi:10.1029/JC090iC03p04741.

Drivdal, M., G. Broström, and K. H. Christensen (2014), Wave-induced mixing and transport of buoyant particles: Application to the Statfjord A oil spill, *Ocean Sci.*, *10*(6), 977–991, doi:10.5194/os-10-977-2014.

Ekman, V. W. (1905), On the influence of the Earth's rotation on ocean-currents, *Ark. Mat. Astron. Fys.*, *2*(11), 1–51.

Elipot, S., and S. T. Gille (2009a), Estimates of wind energy input to the Ekman layer in the Southern Ocean from surface drifter data, *J. Geophys. Res.*, *114*, C06003, doi:10.1029/2008JC005170.

Elipot, S., and S. T. Gille (2009b), Ekman layers in the Southern Ocean: Spectral models and observations, vertical viscosity and boundary layer depth, *Ocean Sci.*, *5*, 115–139, doi:10.5194/os-5-115-2009.

Emery, W., and R. E. Thomson (1997), *Data Analysis Methods in Physical Oceanography*, Elsevier, Amsterdam.

Fontán, A., and B. Cornuelle (2015), Anisotropic response of surface circulation to wind forcing, as inferred from high-frequency radar currents in the southeastern Bay of Biscay, *J. Geophys. Res. Oceans*, *120*, 2945–2957, doi:10.1002/2014JC010671.

Furevik, B. R., and H. Haakenstad (2012), Near-surface marine wind profiles from rawinsonde and NORA10 hindcast, *J. Geophys. Res.*, *117*, D23106, doi:10.1029/2012JD018523.

Gonella, J. (1972), A rotary-component method for analysing meteorological and oceanographic vector time series, *Deep Sea Res.*, *19*, 833–846.

Hasselmann, K. (1970), Wave driven inertial oscillations, *Geophys. Fluid Dyn.*, *1*(3–4), 463–502, doi:10.1080/03091927009365783.

Janssen, P. (2012), Ocean wave effects on the daily cycle in SST, *J. Geophys. Res.*, *117*, C00J32, doi:10.1029/2012JC007943.

Koszalka, I., J. H. LaCasce, and K. A. Orvik (2009), Relative Dispersion in the Nordic Seas, *J. Mar. Res.*, *67*, 411–433, doi:10.1357/002224009790741102.

Kundu, P. K. (1976), Ekman veering observed near the ocean bottom, *J. Phys. Oceanogr.*, *6*, 238–242.

Lewis, D., and S. Belcher (2004), Time-dependent, coupled, Ekman boundary layer solutions incorporating Stokes drift, *Dyn. Atmos. Oceans*, *37*(4), 313–351, doi:10.1016/j.dynatmoce.2003.11.001.

Lumpkin, R., and M. Pazos (2007), Measuring surface currents with surface velocity program drifters: The instrument, its data, and some recent results, in *Lagrangian Analysis and Prediction of Coastal and Ocean Dynamics*, edited by A. Griffa et al., pp. 39–67, Cambridge Univ. Press, New York.

McWilliams, J. C., E. Huckle, J.-H. Liang, and P. P. Sullivan (2012), The wavy Ekman Layer: Langmuir circulations, breaking waves, and Reynolds stress, *J. Phys. Oceanogr.*, *42*, 1793–1816, doi:10.1175/JPO-D-12-07.1.

Monismith, S. G., and D. A. Fong (2004), A note on the potential transport of scalars and organisms by surface waves, *Limnol. Oceanogr.*, *49*, 1214–1217, doi:10.4319/lo.2004.49.4.1214.

Niiler, P. P., and J. D. Paduan (1995), Wind-driven motions in the northeast Pacific as measured by Lagrangian drifters, *J. Phys. Oceanogr.*, *25*, 2819–2830, doi:10.1175/1520-0485(1995)025<2819:WDMITN>2.0.CO;2.

Pazan, S. E., and P. P. Niiler (2001), Recovery of near-surface velocity from undrogued drifters, *J. Atmos. Oceanic Technol.*, *18*, 476–489, doi:10.1175/1520-0426(2001)018<0476:RONSVF>2.0.CO;2.

Polton, J. A., D. M. Lewis, and S. E. Belcher (2005), The role of wave-induced Coriolis-Stokes forcing on the wind-driven mixed layer, *J. Phys. Oceanogr.*, *35*(4), 444–457, doi:10.1175/JPO2701.1.

Poulain, P.-M., R. Gerin, E. Mauri, and R. Pennel (2009), Wind effects on drogued and undrogued drifters in the Eastern Mediterranean, *J. Atmos. Oceanic Technol.*, *26*, 1144–1156, doi:10.1175/2008JTECHO618.1.

Poulain, P.-M., A. Bussani, R. Gerrin, R. Jungwirth, E. Mauri, M. Menna, and G. Notarstefano (2013), Mediterranean surface currents measured with drifters: From basin to subinertial scales, *Oceanography*, *26*, 38–47, doi:10.5670/oceanog.2013.03.

Rascle, N., and F. Ardhuin (2009), Drift and mixing under the ocean surface revisited: Stratified conditions and model-data comparisons, *J. Geophys. Res.*, *114*, C02016, doi:10.1029/2007JC004466.

Reistad, M., O. yvind Breivik, H. Haakenstad, O. J. Aarnes, B. R. Furevik, and J.-R. Bidlot (2011), A high-resolution hindcast of wind and waves for the North Sea, the Norwegian Sea, and the Barents Sea, *J. Geophys. Res.*, *116*, C05019, doi:10.1029/2010JC006402.

Rio, M.-H., and F. Hernandez (2003), High-frequency response of wind-driven currents measured by drifting buoys and altimetry over the world ocean, *J. Geophys. Res.*, *108*(C8), 3283, doi:10.1029/2002JC001655.

Röhrs, J., K. H. Christensen, L. R. Hole, G. Broström, M. Drivdal, and S. Sundby (2012), Observation-based evaluation of surface wave effects on currents and trajectory forecasts, *Ocean Dyn.*, *62*, 1519–1533, doi:10.1007/s10236-012-0576-y.

Röhrs, J., K. H. Christensen, F. B. Vikebø, S. Sundby, Ø. Saetra, and G. Broström (2014), Wave-induced transport and vertical mixing of pelagic eggs and larvae, *Limnol. Oceanogr.*, *59*(4), 1213–1227, doi:10.4319/lo.2014.59.4.1213.

Röhrs, J., A. K. Sperrevik, K. H. Christensen, G. Broström, and Ø. Breivik (2015), Comparison of HF radar measurements with Eulerian and Lagrangian surface currents, *Ocean Dyn.*, *65*(5), 679–690, doi:10.1007/s10236-015-0828-8.

Stokes, G. G. (1847), On the theory of oscillatory waves, *Trans. Cambridge Philos. Soc.*, *8*, 441–473.

Ursell, F. (1950), On the theoretical form of ocean swell on a rotating Earth, *Mon. Not. R. Astron. Soc. Geophys. Suppl.*, *6*, 1–8, doi:10.1111/j.1365-246X.1950.tb02968.x.

Weber, J. E. (1983), Steady wind- and wave-induced currents in the open ocean, *J. Phys. Oceanogr.*, *13*(3), 524–530, doi:10.1175/1520-0485(1983)013<0524:SWAWIC>2.0.CO;2.